2012

Non-Uniform Clearance between Rotor Surfaces and Its Effect on Machine Performance in Twin-Screw Compressors

Hsiang-Hui Hsiao
yuren@mail.npust.edu.tw

Yu-Ren Wu

Ho-Chun Hsieh

Non-Uniform Clearance between Rotor Surfaces and Its Effect on Machine Performance in Twin-Screw Compressors

Hsiang-Hui HSIAO, Yu-Ren WU*, and Ho-Chun HSIEH

Department of Mechanical Engineering, National Pingtung University of Science and Technology, Taiwan, R.O.C.
E-mail: yuren@mail.npust.edu.tw

* Corresponding Author

ABSTRACT

The performance of twin-screw compressors is primarily affected by the clearance between a pair of meshing rotors. This study proposes a method for calculating the normal clearance along the contact line between rotors using two normal rack curves, which are conjugated with the male and female rotors. The clearance distribution results are then compared using the HOLROYD profile management system (HPMS) software to verify their accuracy. Additionally, non-uniform clearance along the contact line between rotor surfaces is included in the compressor performance calculation to assess its influence on the flow leakage and volumetric efficiency.

1. INTRODUCTION

Twin-screw compressors are the core component of cooling and air conditioning systems. They are widely used in medical instruments, food processing machines, and vehicle power systems nowadays. Through the meshing operation of a pair of conjugated male and female rotors inside the compressor housing, the suction, compression, and discharge processes are achieved in the screw channel and the space inside the housing wall. With constant improvements to the design, manufacturing, and analysis, the required precision of the tooth surfaces for twin-screw compressor rotors continues to increase. Clearances that cause high-pressure fluids to leak into the low pressure chamber are also controlled more precisely.

Temperature and high pressure cause potential interferences and abrasions between the tooth surfaces during meshing. Considering the numerous rotor profile design conditions, machining imperfections, and stress deformations and thermal expansions during rotor work, various leakage paths exist. Several important clearances lead to fluid leaks, including (1) clearances in the intertooth contact band, (2) clearances between the rotor suction/discharge ends and the housing end plugs, (3) clearances between the rotor tooth tip and the housing wall, and (4) the blow hole formed between the tips of the teeth of the male and female rotors and the cavity wall. In a twin-screw compressor, sufficient clearance along the contact line must be guaranteed to ensure the safety of the compressor operation. Additionally, the clearance must not be large enough to cause excessive leakage. Litvin and Feng (1997) explored the effect of variations in the rotor axis and rotational angle on the clearance deviation. In his book, Xing (2000) describes methods for obtaining intertooth clearances, including the assembly center distance adjustment method, machining correction method, theoretical profile correction method, and the mixed method.

Traditional clearance measurement methods require significant time and manpower and specific methods or machines. Furthermore, because of analysis software limitations, actual clearance cannot be calculated effectively. Therefore, Huang et al. (2010) used the rotor contact line information from CAD meshing simulations to calculate the clearance distribution along the contact line of rotors using the multiple cross-section iteration method. The primary goal of their study was to develop a method for meshing simulation and clearance calculation to predict actual assembly conditions. Stosic (1998) also developed a computational mathematical model of twin-screw compressor rotor intertooth clearance under assembly error. Xiong (2006) found that clearance designed along the contact line differs significantly from the actual clearance distribution during operation; thus, Xiong proposed an optimization method to provide more precise values when computing contact line clearances.

Previously, tooth profiles were reciprocally generated for male and female rotors. However, as shown by gear principles, a pair of conjugate meshing gears can be generated from the same rack cutter. The normal clearance between gears can be used to calculate the distance from the gear tooth profile along the normal direction to the rack. In his work, Stosic (2005) explained that rotor formation could be regarded as helical gears with nonintersecting axes. He also proposed a method for generating N-type male and female rotor tooth profiles from rack curves. Cavatorta et al. (2011) applied for a patent to protect the male and female rotor tooth profiles generated from racks. Xavier et al. (2011) proposed a design methodology for generating twin-screw compressor rotors from racks, stating that the tooth profiles generated through optimization using this method could effectively improve compressor efficiency. Xiao et al. (2005) explored the clearance for screw surface meshing under conjugate conditions. Seshaiah et al. (2007) performed theoretical modeling of oil-injected screw compressors and examined the leakage paths of screw compressors in the modeling computations. Their modeling results indicated that larger clearances between rotors reduce the volumetric efficiency.

The above studies indicate that theoretically calculated rotor tooth clearances create unpredictable stress deformations in actual operation. Machining error during rotor manufacturing further affects the clearance distribution in the original design. Therefore, for this study, the point data of the measured rotor tooth profiles from 3D CMM are employed to generate rack curves for both male and female rotors using the normal-rack generation method. The normal clearance between the two racks is calculated after positioning. Finally, the calculated non-uniform clearance is distributed into the 3D contact lines to calculate the clearance band area. This can be used to replace the uniform clearance value assumption in previous compressor thermal flow calculations to approach the non-uniform clearance distribution along the contact line more realistically. Subsequently, the amount of leakage through the clearance band and the effects of non-uniform clearance distribution on the compressor efficiency can also be calculated more realistically.

2. GENERATION OF NORMAL RACK PROFILES

Because the 3D CMM measurement point data of rotor profiles are used as the input for clearance calculations in this study, curve fitting must be performed before normal rack curve and clearance calculations. In this study, we use cubic spline to fit the discrete tooth profile points on the male and female rotors. After fitting, the general equation $\boldsymbol{r}(u)$ for the various fitted curve sections of the rotor tooth profile is shown below.

$$\boldsymbol{r}(u) = [x(u),\ y(u)] = [\sum_{k=0}^{3} c_{k,x} u^k,\ \sum_{k=0}^{3} c_{k,y} u^k],\ 0 \le u \le u_s \tag{1}$$

where u is the profile parameter for each segment of fitted curves (rotor tooth profile direction parameter), u_s is the upper limit of the profile parameters for the equations of each fitted segment and the chord length between adjacent points, $c_{k,x}$ and $c_{k,y}$ are the coefficients of the curve fitting equations $x(u)$ and $y(u)$, respectively, and k is the order of the fitting equation (k = 0 ~ 3). Therefore, in the above equation, if m instances of data exist for the rotor tooth profile discrete point data, ($m-1$) fitting equations also exist.

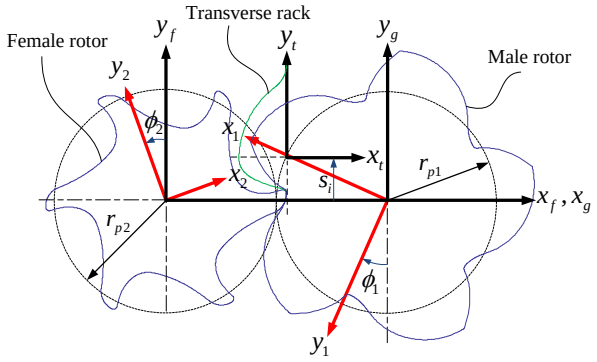

Figure 1: Coordinate systems for the male and female rotors and the transverse rack

The gear meshing principle indicates that two gears generated by the same rack cutter conjugate each other. According to this principle, the fitted rotor tooth profile equation can be used to determine the equations for the rack. The relative motion coordinate systems for male and female rotors and the rack are shown in Figure 1, where S_1 and S_2 represent the rotation coordinate systems affixed to the male rotor and the female rotor, respectively, S_t represents the translational coordinate system affixed to the transverse rack, and S_f and S_g represent the fixed coordinate systems.

In coordinate systems S_1 and S_2, the fitted tooth profile equations for the male and female rotors $\mathbf{r}_1$ and $\mathbf{r}_2$, the normal vectors $\mathbf{N}_1$ and $\mathbf{N}_2$, and the unit normal vectors $\mathbf{n}_1$ and $\mathbf{n}_2$ can be represented as follows:

$$\mathbf{r}_i(u) = [x_i(u), y_i(u), 1]^T,\ i = 1,2 \tag{2}$$

$$\mathbf{N}_i(u) = \mathbf{k} \times \frac{\partial \mathbf{r}_i}{\partial u};\ \mathbf{n}_i(u) = \frac{\mathbf{N}_i(u)}{\sqrt{\mathbf{N}_i(u) \cdot \mathbf{N}_i(u)}},\ i = 1,2 \tag{3}$$

where the superscript T indicates the transpose matrix, $\mathbf{k} = [0,0,1]$ is the unit vector along z-axis, subscript $i = 1$ represents the male rotor, and subscript $i = 2$ represents the female rotor.

From the motion relationships between the rack and the male/female rotor, we can determine the locus equation $\mathbf{r}_{ti}$ and the unit normal vector $\mathbf{n}_{ti}$ of the male/female rotor tooth profile in the coordinate system S_t, as shown below.

$$\mathbf{r}_{ti}(u, \phi_i) = \mathbf{M}_{ti}(\phi_i) \cdot \mathbf{r}_i(u),\ i = 1,2 \tag{4}$$

$$\mathbf{n}_{ti}(u, \phi_i) = \mathbf{M}_{ti}(\phi_i) \cdot \mathbf{n}_i(u),\ i = 1,2 \tag{5}$$

$$\mathbf{M}_{ti} = \begin{bmatrix} 1 & 0 & (-1)^{i-1} r_{pi} \\ 0 & 1 & -s_i \\ 0 & 0 & 1 \end{bmatrix} \cdot \begin{bmatrix} \cos\phi_i & (-1)^{i-1}\sin\phi_i & 0 \\ (-1)^{i}\sin\phi_i & \cos\phi_i & 0 \\ 0 & 0 & 1 \end{bmatrix},\ i = 1,2 \tag{6}$$

where $s_i = r_{pi}\phi_i$ and r_{pi} is the pitch radius of the male/female rotor, ϕ_i is the rotation angle of the male/female rotor, and $\mathbf{M}_{ti}$ is the coordinate transformation matrix from S_i to S_t.

To obtain the relationship equation between the profile parameter u and the rotation angles ϕ_1 and ϕ_2, we derive the equation of meshing with the necessary condition that the common normal vector at the contact point is perpendicular to the relative velocity between two conjugate curves, as shown below.

$$f_i(u, \phi_i) = \mathbf{n}_{ti} \cdot \partial_{\phi_i} \mathbf{r}_{ti} = 0,\ i = 1,2 \tag{7}$$

Substituting the u value from each fitted curve segment of the male and female rotors into Equation (7) yields the corresponding rotation angle value ϕ_i. By substituting this back into Equations (4) and (5), we can obtain the corresponding transverse rack coordinates and unit normal vectors for each point for the male and female rotors.

The normal rack equation $\mathbf{r}_{ni}$ can be derived by projecting the transverse rack onto the normal cross-section:

$$\mathbf{r}_{ni} = [x_{ti}, y_{ti}\cos\beta, 1],\ i = 1,2 \tag{8}$$

$$\mathbf{N}_{ni}(u)=\frac{\partial \mathbf{r}_{ni}}{\partial u}\times\mathbf{k};\ \mathbf{n}_{ni}(u)=\frac{\mathbf{N}_{ni}(u)}{\sqrt{\mathbf{N}_{ni}(u)\cdot\mathbf{N}_{ni}(u)}},\ i=1,2 \tag{9}$$

where β is the pitch helix angle of the rotor, and $\mathbf{n}_{n1}$ and $\mathbf{n}_{n2}$ are the unit normal vector equations for the normal rack of the male and female rotors, respectively.

3. NORMAL CLEARANCE CALCULATION PROCEDURE

Figure 2 is a flowchart of the calculation process for the normal clearance between the tooth surfaces of the male and female rotors in this study. First, 3D measurement tooth profile point data are imported into the developed program. Then, points are deleted, interpolated, and relocated during the preprocessing of point data. Next, the method described in the previous section is used to determine the normal rack curve for the male and female rotors. Subsequently, the normal clearance is calculated using the two normal rack curves. After the normal clearances for each point on the normal rack curve are obtained, the processed normal rack can be used to determine the 3D contact point coordinates. The clearances are distributed onto the contact points to draw the 3D spatial contact line clearance distribution graph. Finally, variations in the contact band area following the male rotor rotation angle are calculated and then used to conduct compressor performance modeling computations. This provides the amount of leakage through the contact band and the volumetric efficiency. The procedures for each step are explained below.

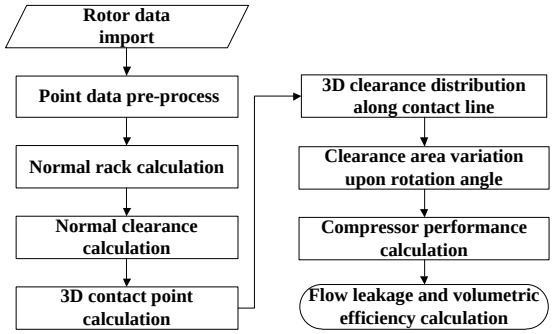

Figure 2: Flowchart of normal clearance calculations

3.1 Pre-process of Measured Rotor Profile Data

Because the measured rotor tooth profile point data often contain extra points and are shown as the tooth groove, duplicate points must be deleted and the entire series rearranged. As shown in Figure 3, the radius value for each point on the male rotor tooth profile is first calculated. The sequence number of the point with the least radius value is used to divide the left and right halves of the male rotor tooth profile information. The left half of the male rotor profile information is then rotated to a ($2\pi / z_1$) angle (where z_1 is the tooth number of the male rotor). After the point data are rearranged, the male and female rotor tooth profiles are positioned on the horizontal axis.

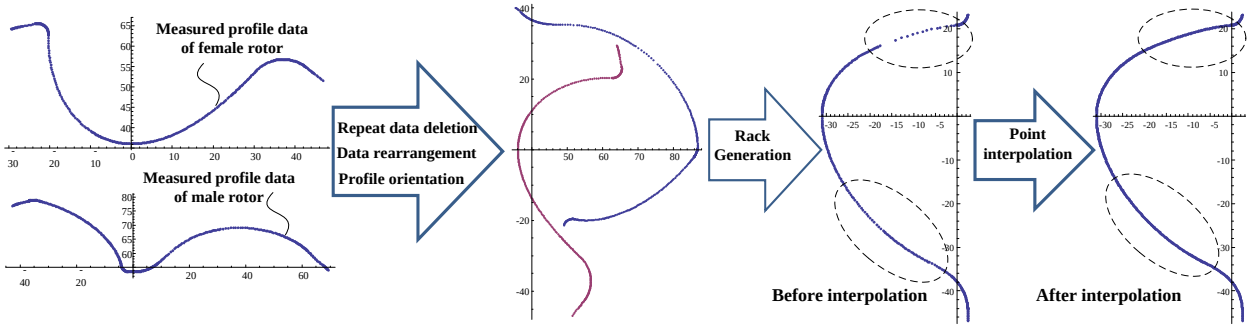

Figure 3: Point data pre-process and interpolation

3.2 Generation of Normal Rack Profiles

After the processing described in Section 3.1, the male and female rotor tooth profile point data are fitted with cubic splines. The mathematical models described in Section 2 can be used to obtain rack curves that correspond to the male and female rotors. To ensure that the subsequent clearance distribution is homogenous, we calculated the point distance for each point and then used these data to conduct interpolation computations. The rotor tooth profile points after interpolation are shown in Figure 3.

Figure 4 shows the normal and transverse sections of rotors and the normal racks can be projected from the transverse rack curves of the male and female rotors. The solid curve is the normal rack profile of the female rotor, and the dotted curve is the normal rack profile of the male rotor. After assembly based on the enlarged assembly center distance, the amount of clearance between the two normal rack curves is visible from the graph.

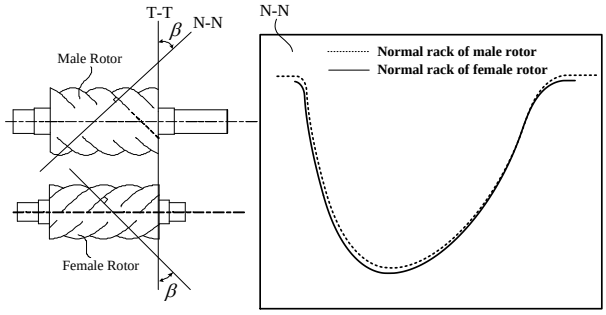

Figure 4: Normal rack profiles of male and female rotors

3.3 Normal Clearance Calculation

As shown in Figure 5, we used each point on the normal rack of the female rotor as a standard and computed the normal clearance from each point on the female rotor normal rack to the male rotor normal rack. To reduce the computation time, we had to first determine the point interval in the male rotor normal rack that the unit normal vector of each point on the female rotor normal rack passed through. Where $\mathbf{r}_{n2}^{(j)}$ is the position of a certain point j on the normal rack of the female rotor ($j=1\sim m_2$, m_2 is the number of points on the female rotor normal rack), $\mathbf{r}_{n1}^{(i)}$ and $\mathbf{r}_{n2}^{(i+1)}$ are the positions of a certain point i on the male rotor normal rack and its next point $i+1$ ($i=1\sim m_1$, m_1 is the number of points on the male rotor normal rack), and $\mathbf{n}_{n2}^{(i)}$ is the unit normal vector of point $\mathbf{r}_{n2}^{(i)}$. When the following condition is satisfied, the unit vector $\mathbf{n}_{n2}^{(j)}$ passes though the point interval [*i*, *i+1*] on the male rotor normal rack.

$$(\mathbf{a}_1\times\mathbf{n}_{n2}^{(j)})\cdot(\mathbf{a}_2\times\mathbf{n}_{n2}^{(j)})<0 \tag{10}$$

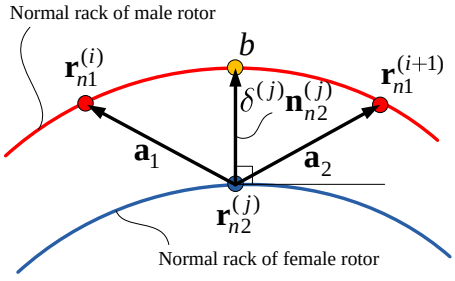

Figure 5: Schematic chart for calculating the normal clearance section

Subsequently, each point on the female rotor normal rack is substituted into Equation (11) to obtain the normal clearance $\delta^{(j)}$ between each point on the female rotor normal rack $\mathbf{r}_{n2}^{(j)}$ and the male rotor normal rack.

$$\mathbf{r}_{n2}^{(j)} + \delta^{(j)}\mathbf{n}_{n2}^{(j)} - \mathbf{r}_{n1}(u) = 0 \tag{11}$$

Drawing the normal clearance $\delta^{(j)}$ in the normal direction of each point along the female rotor normal rack sequentially provides the female rotor rack clearance graph.

3.4 Normal Clearance Distribution along the 3D Contact Line

After the clearance value for each point along the normal rack is obtained, the female rotor normal rack point data after interpolation are fitted with cubic splines as equation $\mathbf{r}_{n2}(u)$, $u = 0 \sim u_s$ and then projected back to the transverse section to yield the transverse rack equation $\mathbf{r}_{t2}(u)$ and calculate its unit normal vector $\mathbf{n}_{t2}(u)$.

$$\mathbf{r}_{t2}(u) = [x_{n2}(u), y_{n2}(u)/\cos\beta, 1] \tag{12}$$

$$\mathbf{N}_{t2}(u) = \mathbf{k} \times \frac{\partial \mathbf{r}_{t2}}{\partial u};\ \mathbf{n}_{t2}(u) = \frac{\mathbf{N}_{t2}(u)}{\sqrt{\mathbf{N}_{t2}(u) \cdot \mathbf{N}_{t2}(u)}} \tag{13}$$

According to the relative motion coordinate system shown in Figure 1, the female rotor tooth profile Equation $\mathbf{r}_2(u, \phi_2(u))$ and its corresponding meshing rotation angle ϕ_2 for the transverse rack in S_2 can be obtained using the coordinate transformation matrix $\mathbf{M}_{2t}$ and equation of meshing $f_{2t}(u, \phi_2) = 0$, as shown below.

$$\mathbf{r}_2(u, \phi_2) = \mathbf{M}_{2t}(\phi_2) \cdot \mathbf{r}_{t2}(u) \tag{14}$$

$$\mathbf{n}_2(u, \phi_2) = \mathbf{M}_{2t}(\phi_2) \cdot \mathbf{n}_{t2}(u) \tag{15}$$

$$\mathbf{M}_{2t}(\phi_2) = \begin{bmatrix} \cos\phi_2 & \sin\phi_2 & 0 \\ -\sin\phi_2 & \cos\phi_2 & 0 \\ 0 & 0 & 1 \end{bmatrix} \cdot \begin{bmatrix} 1 & 0 & r_{p2} \\ 0 & 1 & s_i \\ 0 & 0 & 1 \end{bmatrix} \tag{16}$$

$$f_2(u, \phi_2) = \mathbf{n}_2 \cdot \partial_{\phi_2} \mathbf{r}_2 = 0 \tag{17}$$

The female rotor tooth profile equation $\mathbf{r}_2(u, \phi_2(u))$ and meshing rotation angle ϕ_2 can be introduced into the following equation to yield the contact line equation $\mathbf{r}_f$ under the fixed coordinate system.

$$\mathbf{r}_f = [x_f, y_f, z_f] = [x_2\cos\phi_2 + y_2\sin\phi_2, -x_2\sin\phi_2 + y_2\cos\phi_2, p_2\phi_2] \tag{18}$$

where $p_2 = r_{p2}\cot\beta$ is the female rotor helix parameter.

After the profile parameter *u* at each point is substituted into Equation (18), the corresponding contact line point coordinate $\mathbf{r}_f^{(j)}$ can be obtained. By multiplying the normal vector on each point of the contact line $\mathbf{n}_{n2}^{(j)}$ with the normal clearance value $\delta^{(j)}$, we can obtain the normal clearance distribution of the 3D contact line.

$$[x_c^{(j)}, y_c^{(j)}, z_c^{(j)}] = [x_f^{(j)} + n_{n2,x}^{(j)}\delta^{(j)}, y_f^{(j)} + n_{n2,y}^{(j)}\delta^{(j)}, p_2\phi_2],\ j = 1 \sim m_2 \tag{19}$$

4. NUMERICAL EXAMPLES

To validate the normal clearance calculation (NCC) process established in this study, the N4 rotor tooth profile offered by a large compressor manufacturer was used in Example 4.1 to calculate the normal clearance distribution

for the N4-type rotor tooth profile from two clearance designs. The results were compared with the analyzed clearance values from the well-known Holroyd profile management system (HPMS) rotor machining software. The N4-type rotor tooth profile was also used in Example 4.2, and the results were compared with those provided by HPMS. The only difference was the contact positions between the male and female rotors analyzed. In Example 4.3, the N4-type rotor tooth profile (Case B) was used to calculate variations of the clearance area along the contact line regarding the male rotor rotation angle, and compressor performance was determined. This was used to compare the effects of the uniform and non-uniform clearance contact bands on the leakage and volumetric efficiency of the compressors. Table 1 shows the geometric parameters of N4-type rotors.

Table 1: Geometric parameters of N4-type rotors

Items (Units)	Male Rotor	Female Rotor
Tooth Number	5	6
Assembly Center Distance (mm)	82.0	
Helix Angle (degree)	46.0	
Rotor Screw Length (mm)	108.32	
Inner Radius/Outer Radius (mm)	35.67/ 57.95	24.05/ 46.33

4.1 Clearance Calculation for N4 Rotors with Differing Clearance Designs

First, the N4-type rotor tooth profile with clearance design A was used to conduct clearance analysis calculations. In this example, the two rotors are contacting at the driving side tooth surface pitch circle, which is used for clearance calculations. As shown in Figure 6, the maximum clearance calculated using the program developed in this study (NCC) was 0.169 mm, with a single tooth clearance band area of 13.478 mm^2. The clearance graph analysis provided by the well-known rotor machining software HPMS is also shown in Figure 6. The maximum clearance is 0.1686 mm, with a single tooth clearance band area of 13.525 mm^2. As shown in Table 2, NCC and HPMS show a 0.24% error percentage in the maximum clearance amount, and a 0.35% error percentage in the single tooth clearance band area. By comparing the normal clearance distribution between the two methods using line charts, we found that the clearance distribution curves were generally identical (in the NCC results graph, the horizontal axis is the point sequence number and the vertical axis is the normal clearance value; in the HPMS results graph, the horizontal axis is the contact line length percentage and the vertical axis is the normal clearance value). This verifies the reliability and accuracy of the computational method and program developed in this study. Right graph in Figure 6 shows the clearance computation results along 3D contact lines presented on z-y plane.

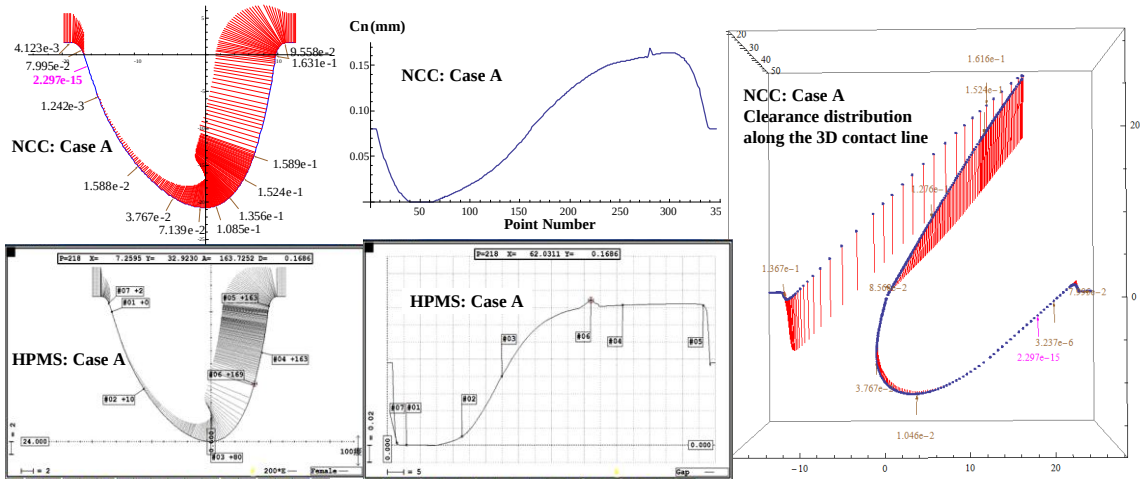

Figure 6: Comparison of the normal clearance distribution between NCC and HPMS for N4 rotor profiles (Case A)

Second, the N4-type rotor tooth profile with clearance design B was used to analyze clearance calculations. In this example, the two rotors are contacting at the left side of the tooth surface pitch circle, which is used for clearance calculations. As shown in Figure 7, the maximum clearance calculated from the program developed in this study (NCC) was 0.0878 mm, with a single tooth clearance band area of 10.207 mm^2. Figure 7 also shows the clearance

graph analyzed using the HPMS software. The maximum clearance was 0.0959 mm, with a single tooth clearance band area of 9.835 mm^2. As shown in Table 2, NCC and HPMS show an 8.45% error percentage in the maximum clearance amount, and a 3.78% error percentage in the single tooth clearance band area. This indicates that the errors involved in clearance design B are larger than those in clearance design A. Because of the differing methods of processing the rotor tooth profile point data, and the fact that the defined contact points show some differences, the calculated values contain certain errors. However, by comparing the normal clearance distribution between the two methods using line charts, we found that the clearance distribution curves are generally the same. Right graph in Figure 7 shows the clearance computation results along 3D contact lines presented on z-y plane.

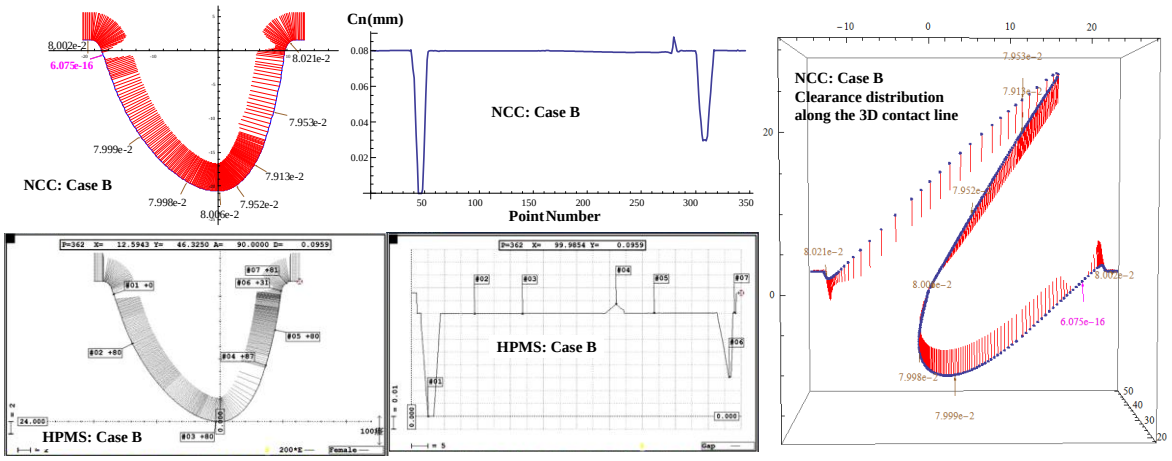

Figure 7: Comparison of the normal clearance distribution between NCC and HPMS for N4 rotor profiles (Case B)

Table 2: Clearance calculation comparison between NCC and HPMS for Cases A and B on different contact sides

N4 Rotor on driving contact sides (Case A)	**NCC**	**HPMS**	**Error (%)**
Max. Normal Clearance (mm)	0.1690	0.1686	0.24
Area of Clearance Band (mm^2)	13.478	13.525	0.35
N4 Rotor on driving contact sides (Case B)	**NCC**	**HPMS**	**Error (%)**
Max. Normal Clearance (mm)	0.0878	0.0959	8.45
Area of Clearance Band (mm^2)	10.207	9.835	3.78
N4 Rotor on driven contact sides (Case B)	**NCC**	**HPMS**	**Error (%)**
Max. Normal Clearance (mm)	0.1095	0.1101	0.54
Area of Clearance Band (mm^2)	9.235	8.658	6.66

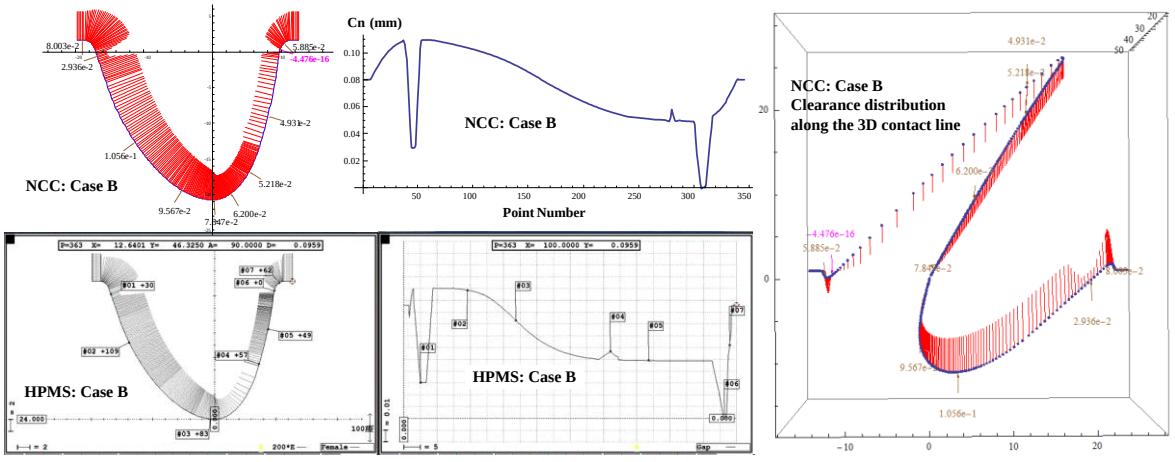

Figure 8: Comparison of the normal clearance distribution between NCC and HPMS for N4 rotor profiles on driven contact sides (Case B)

4.2 Clearance Calculations for N4 Rotors on Different Contact Sides

In this example, point information from the N4-type rotor tooth profile with clearance design B was used to analyze clearance calculations. The contact position between the two rotors was defined at the driven side tooth surface pitch circle, which is used for clearance calculations to validate the accuracy of the clearance distribution results of various contact positions. As shown in Figure 8, the maximum clearance calculated by the program developed in this study (NCC) was 0.1095 mm, with a single tooth clearance band area of 9.235 mm^2. The maximum clearance analyzed using the HPMS was 0.1101 mm, with a single tooth clearance band area of 8.658 mm^2. As shown in Table 2, NCC and HPMS have a 0.54% error percentage in the maximum clearance amount and a 6.66% error percentage in the single tooth clearance band area. By comparing the normal clearance distribution between the two methods using line charts, we found that the clearance distribution curves were generally the same. This demonstrates the reliability and accuracy of the computational method and program developed in this study. Right graph in Figure 8 shows the clearance computation results along 3D contact lines presented on z-y plane.

4.3 Difference in Compressor Performance between Uniform and Non-Uniform Clearance

The amount of leakage between the compressor rotors through the contact line clearance band was previously calculated using uniform clearance to determine the leakage area, which was then further used to calculate the mass flow rate of leakage through the contact line. In this example, we go beyond previous studies and use a non-uniform normal clearance area value and its variations along the male rotor rotation angles to model the leakage mass flow rate of the compressor through the contact line. Furthermore, we compare the compressor performance calculation results of uniform clearance with those of non-uniform clearance.

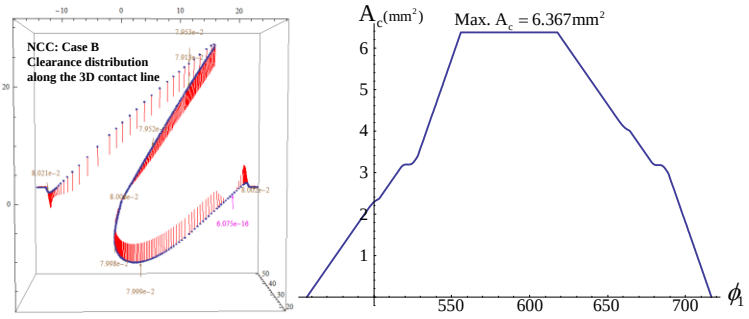

Figure 9: Variation curve of the normal clearance area and the male rotor rotation angle

First, the normal clearance calculation results for the 3D contact line from the N4-type rotor tooth profile under clearance design B were used and yielded the variation curve and data for the normal clearance band area A_c and the male rotor rotation angle ϕ_1. These were used as input data to calculate the effect of non-uniform clearance on performance, as shown in Figure 9. The overall average clearance of 0.0763 mm was calculated and used as the input for calculations regarding the effect of the uniform clearance design on performance to facilitate performance comparisons between uniform and non-uniform clearance calculations. The operational condition parameters adopted for the compressor thermal flow performance modeling computation programs are shown in Table 3.

Table 3: Operating conditions for determining the compressor performance

Items (Units)	Values
Operating Rotation Speed (rpm)	3550
Input Power (HP)	45.0
Volume Ratio	4.411
Calculated Uniform Clearance (mm)	0.076
Rotor Tip and Housing Clearance (mm)	0.08
Suction/Discharge End Clearance (mm)	0.25/ 0.05
Inlet/Discharge Pressure (Pa)	3.626×10^5 / 9.278×10^5

The comparison results of the compressor thermal flow performance modeling shown in Table 4 indicate that the leakage area for non-uniform clearance is smaller than that for the uniform clearance area, which reduces the mass

flow leakage rate through the contact line by 17.74% and increases the volumetric efficiency of the compressor by 0.779%. Therefore, the previous performance results calculated using uniform clearances show greater differences from actual conditions.

Table 4: Comparison of the compressor performance indices between uniform and non-uniform clearances

Items (Units)	Uniform Clearance	Non-Uniform Clearance	Difference (%)
Theoretical Max. Flow Rate, V_1 (kg/s)	2519.377	2519.377	—
Calculated Flow Rate, V_2 (kg/s)	2183.741	2200.749	—
Volumetric Efficiency, V_2/V_1	0.867	0.874	0.779 %
Leakage Through Contact Clearance Band (kg)	9.36×10^{-5}	7.7×10^{-5}	-17.74%

6. CONCLUSIONS

This study proposed a method for calculating the normal clearance between rotor tooth surfaces by using the normal racks derived from male and female rotor profiles. Based on the numerical calculation examples, the achievements of this study are summarized as follows:

1. The complex calculation of clearance between 3D male and female rotor teeth surfaces along the contact line can be transformed into a simple clearance calculation between planar normal racks.
2. The accuracy of the clearance calculations in this study was verified through comparisons with the clearance values provided by HPMS software.
3. Changes in the non-uniform clearance area along the 3D contact line between the rotor tooth surfaces based on the rotation angle of the male rotor were used to approach a more realistic condition and to replace previous calculations of leakage and volumetric efficiencies (within compressor performance determinations) that assumed uniform clearance.
4. The leakage amount calculated using non-uniform clearances is lower than that of uniform clearances and volumetric efficiencies are higher, which has a substantial effect on performance calculation results.

REFERENCES

Xing, Z.W., 2000, Screw Compressors: Theory, Design and Application, *China Machine Press*, Beijing, China. (in Chinese)

Litvin, F.L., Feng, P.H., 1997, Computerized Design, Generation, and Simulation of Meshing of Rotors of Screw Compressor, *Mechanism and Machine* Theory, vol. 32, no. 2: p. 137-160.

Stosic, N., 1998, On Gearing of Helical Screw Compressor Rotors, *Proceedings of the Institution of Mechanical Engineers*, Part C: Journal of Mechanical Engineering Science, vol. 212: p. 587-594.

Xiao, D.Z., Gao, Y., Wang, Z.Q., Liu, D.M., 2005, Conjugation Criterion for Making Clearance of the Meshed Helical Surfaces, *Journal of Mechanical Design*, vol. 127, issue 1: p. 164-168.

Stosic, N., Smith, I., Kovacevic, A., 2005, Screw Compressors: Mathematical Modeling and Performance Calculation, *Springer Verlag*, New York.

Xiong, W., 2006, Calculation on the Inter-Lobe Clearance Distribution of Twin-Screw Compressor by Optimization Method, *International Compressor Engineering Conference at Purdue*, C020: p. 1-8.

Seshaiah, N., Ghosh, S.K., Sahoo, R.K., Sarangi, S.K., 2007, Mathematical Modeling of the Working Cycle of Oil Injected Rotary Twin Screw Compressor, *Applied Thermal Engineering*, vol. 27: p. 145-155.

Huang, Y.C., Lai, J.Y., Lin, F.Y., Guo, Y.L., 2010, Two-Dimensional Localization and Clearance Evaluation of Screw Rotors, *Int. J. Computer Applications in Technology*, vol. 37, no. 1: p. 74-85.

Xavier, P.J., Kanthavel, K., Mythili, R.U., 2011, Rotor Profile Design for Twin Screw Compressor, *International Journal of Scientific & Engineering Research*, vol. 2, Issue 7: p. 1-4.

Cavatorta, P., Tomei, U., 2011, Screw Compressor, *U.S. patent*, no. 0189044.

ACKNOWLEDGEMENT

The authors thank National Science Council (NSC 100-2622-E-194-006-CC2) and HANBELL Precise Machinery Co., Ltd for providing financial and equipment support in Taiwan, Republic of China.